POAC'23
Glasgow, United Kingdom

Proceedings of the 27th International Conference on
Port and Ocean Engineering under Arctic Conditions
12-16 June 2023, Glasgow, United Kingdom

High-speed Impact Drop Tower Tests of Cylindrical Granular Ice Specimens

Angelo Mario Böhm[1], Franciska Müller[1], Hauke Herrnring[1], Franz von Bock und Polach[1]

[1] Hamburg University of Technology, Hamburg, Germany

ABSTRACT

Global warming might increase the marginal ice zone, and it increases the accessibility of the Northern Sea Route and the Northwest Passage for the shipping industry, which reduces the shipping time and fuel consumption in comparison to the Suez Canal Route on single voyages. Thus it is presumed that global warming will enlarge the area of possible propeller-ice and wave-ice structure interactions with ships and structures of lower ice classes or less ice strengthening. The interaction velocities between ice and marine structures are often relatively slow, but some scenarios have high relative interaction velocities, such as in propeller-ice interactions. However, experimental data and knowledge on the mechanical behavior in the high-velocity range of ice are scarce.

This paper describes high-speed impact drop tower tests of cylindrical granular ice specimens, where adjusting the initial drop height can regulate the impact energy level. Depending on the prevailing conditions, sea ice growth can result in several different grain structures. This study utilizes granular fresh water ice, which allows consistency and repeatability of the mechanical behavior and results in conservatively (high) measured compressive strength values compared to saline sea ice. Two test cases are shown and analyzed. In the first case, the hammer impacts the ice specimen positioned on the measuring platform. In the second case, the specimen is also positioned on the measuring platform, but rubber plates are placed between the hammer, the ice specimen, and the measuring platform. All test cases are conducted at three different impact velocities. Force-displacement curves are shown besides high-speed recordings to distinguish between failure modes, and the influence of the end-cap conditions by using rubber plates is discussed. In addition, the paper compares the data from drop tower tests to conventional ice compression tests. This study highlights the impact of boundary conditions and seeks to contribute to developing numerical ice material models for a more economical and safer design of structures in ice, expecting high-speed interactions with ice.

KEY WORDS: Compressive strength, high strain-rates, stress boundary conditions, propeller-ice interaction, ice experiments

INTRODUCTION

Measured ice strength values are influenced by various intrinsic factors such as temperature, salinity, density, ice type, crystal size, and orientation, as well as by test conditions, including strain-rate, confinement conditions, loading direction, sample size, stiffness of the test machine, and sample preparation technique (Timco & Weeks, 2010).

Hawkes and Mellor (1970) presented the difference between idealized and actual test conditions for uniaxial compression tests of rocks. They highlighted the importance of the boundary conditions on the measured compressive strength. In addition, Hawkes and Mellor (1972) found that high tolerances at the surface of the specimen ends and at the platen surface caused an apparent decrease in compressive strength during ice compression tests in the brittle range. The measured strength was lower for cylindrical specimens than for dumbbell specimens, regardless that the ends of the cylindrical specimens were faced off in a lathe. In the study of Haynes and Mellor (1977), ice specimens with saw-cut and lapped ends exhibited a 3 % difference in strength compared to the ice specimens tested with urethane platens. According to their findings, these platens can reduce stress concentrations due to surface irregularities. These results agree with the recommendation made by the working group of the IAHR Section on Ice Problems (Schwarz *et al.*, 1981), which proposes the use of compliant plates as a practical testing alternative for uniaxial compression testing of ice. Schulson (1987; Schulson *et al.*, 1989; Schulson, 1990) suggested for strain-rates between 10^{-3}-10^{-1} s^{-1} that the compressional end-constraint arising from the use of synthane end-caps bonded to the ice increases the brittle compressive strength (shear faulting) and, without this constraint, the fracture would probably occur through axial splitting.

Cole (1987) studied the strain-rate effect in the strain-rate range from 10^{-2} to 10^{-1} s^{-1} in uniaxial ice testing and measured compressive strength values around 5 MPa and concluded that the measured strength is independent of the strain-rate. In contrast, Jones (1997) showed that the compressive strength of columnar ice continues to increase from 6 MPa to 15 MPa in the strain-rate range 10^{-1} – 10^{1} s^{-1}, at -11°C. Fasanella *et al.* (2006) used a drop tower and measured an increased average strength from 5.185 MPa to 6.943 MPa for single crystal or multiple columnar crystal ice tests in the strain-rate range of 107 s^{-1} to 295 s^{-1} and stated that the ice behaved more like a fluid. Shazly *et al.* (2009) used a modified split Hopkinson pressure bar (SHPB) to investigate the dynamic response of ice under uniaxial compression in the range of strain-rates from 60 to 1400 s^{-1} and at initial test temperatures of -10 °C and -30 °C. The compressive strength of ice (9.5 MPa – 58.4 MPa, depending on the tested grain structure and specimen dimension) increased with increasing strain-rates. In addition, Shazly *et al.* (2009) stated that the effect of specimen end-constraint is negligible.

This paper intends to provide information on whether the compressive strength of cylindrical granular ice specimens increases with increasing strain-rates using a drop tower, as the literature has been contradictory in some cases in the past. The literature from (Hawkes & Mellor, 1970; Hawkes & Mellor, 1972; Haynes & Mellor, 1977; Schwarz *et al.*, 1981; Schulson, 1987; Schulson *et al.*, 1989; Schulson, 1990) highlights that compression tests of brittle materials are highly dependent on boundary conditions. Thus the authors also investigate the influence of steel-ice and rubber-ice contact conditions on the failure mode of ice. In propeller-ice interactions, high velocities and different contact conditions are present, which is also attributed to the compliance of the propeller blade. In existing models (Veitch, 1995; Soininen, 1998) , the propeller blade is modeled as a rigid body, and whether the compressive strength fits the scenario is not further specified. Consequently, the results of this paper, in combination with the literature, aid the development of numerical ice material models for propeller-ice interaction simulations.

EXPERIMENTS

In the following, the preparation and execution of the experiments are described, and the test matrix is introduced.

Specimen production and preparation

The ice specimens used for the experiments were cylindrical, with a diameter of 99.4 mm. The ice specimen production process is based on Gudimetla *et al.* (2012), but commercial crushed ice was used instead of self-made crushed ice. For the freezing process of the ice specimens, PVC-U pipes were used, which were sealed at the bottom with a thin aluminum plate and insulated at the top. This ensured freezing from bottom to top and avoided cracking during the freezing process. The forms were filled with 1/3 distilled water and 2/3 commercially available crushed ice to obtain a granular grain structure of the ice. The ice specimens were prepared and frozen in a refrigerated container at -10 °C. The freezing time was two days. After freezing, the ice specimens were removed from the pipes under ambient conditions in the laboratory and again stored in the refrigerated container at -10 °C, where they were shortened to 250 mm in length with a band-saw. Beyond this, the ice specimens did not receive any further treatment.

Experimental Setup

The experiments are conducted at the *Institute of Ship Structural Design and Analysis* laboratory at the *Hamburg University of Technology*. The experiments were conducted on a drop tower to realize high interaction velocities in the experiments, shown in Figure 1.

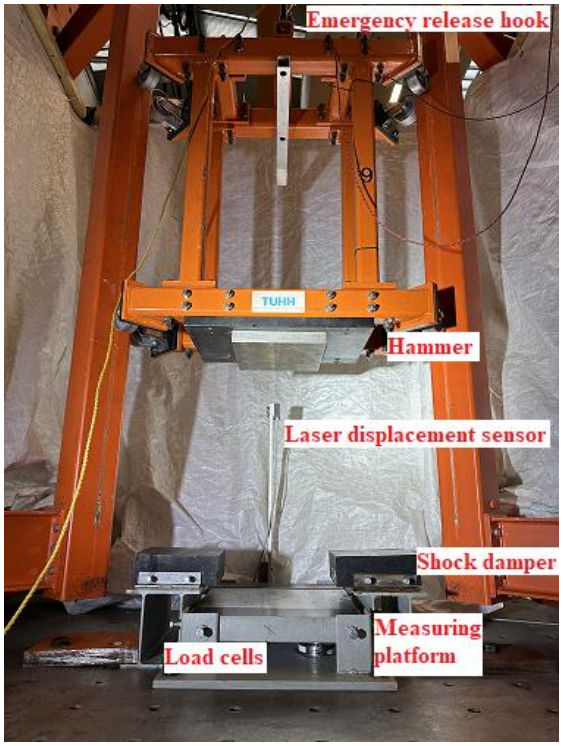

Figure 1: Drop tower at the *Institute of Ship Structural Design and Analysis* of the *Hamburg University of Technology*

The ice specimens were placed on the measuring platform centered underneath the drop hammer. An emergency release hook released the vertically guided drop hammer from a predefined height and hit the ice specimen. A laser displacement sensor measured the movement of the drop hammer during the tests. Four load cells of type *Sartorius PR 6251/14 PanCake Level Sensor* measured the load, which were positioned underneath the measuring

platform. The displacement, and load signal were measured at a sampling rate of 100 kHz. Shock dampers stopped the hammer and protected the load cells by absorbing the residual energy after the compression of the ice. A high-speed camera was utilized to analyze the failure behavior of the ice specimens. It was triggered automatically, and the pictures were stored until the ring memory was full. The recordings were conducted in a frame rate of 10,000 frames per second (fps) to 12,000 fps, which resulted in about 30 pictures of the impact/failure process.

Test Matrix

Two test parameters were varied in the experiments: the end-cap conditions (boundary conditions) and the test velocity. The different velocities were achieved by adjusting the drop height of the hammer. The end-cap conditions consisted of steel-ice contact conditions and rubber-ice contact conditions. It was presumed that the alignment of hammer and specimen was not fully parallel due to practical limitations. To compensate for this effect and the effect of the flatness of the specimen's ends, rubber plates of type *NR/SBR* with a shore hardness of 40 +/-5 Shore A (*Semperit A560*) and a thickness of 3 mm are placed between the hammer, the ice specimen, and the measuring platform by double-sided tape. The length and width of the rubber plate were about 200 mm. The rubber plates were replaced every 2-3 test runs because the surface irregularities at the specimen's ends damaged the rubber plates.

The test matrix in Table 1 shows the end-cap conditions, the number of tests for each series, and the nominal velocity, v_n.

Table 1. Test Matrix

End-cap condition	No. of tests	v_n [mm/s]
Steel-ice	5	3,132
Steel-ice	5	5,425
Steel-ice	5	6,185
Rubber-ice	5	3,132
Rubber-ice	14	5,425
Rubber-ice	14	6,185

The nominal velocity is determined analytically for the free-falling hammer under gravity by considering the principle of conservation of energy as follows:

$$E = mgh = \frac{1}{2}mv^2 = constant \quad (1)$$

$$v_n = \sqrt{2gh} \quad (2)$$

RESULTS

Two different test series have been conducted containing different end-cap conditions and interaction velocities. Each test series followed the objective of investigating the influence of the end-cap condition and the interaction velocity on the measured force. The following sections show the results of the measurements and the high-speed recordings and their analysis.

Measurements

Figure 2 shows four graphs. From top to bottom, the unprocessed displacement-time measurement, the force-time measurement, the force-time history between the time of the first local maxima and the second local minima of the unprocessed displacement-time measurement, and lastly, a detailed representation of the measured force during impact for the test at maximum nominal impact velocity with steel-ice contact is shown. The force measurement from the four load cells connected to the measuring platform was summed (second to fourth graph). The first graph shows that the laser displacement sensor has a maximum measuring length of 750 mm so that the starting movement of the hammer is not measured. Thus the measurement shows zero values until the hammer falls into the possible measuring length of the sensor. At the second local minima, the shortly before absorbed energy of the shock dampers is introduced into the hammer, and the hammer starts to move up. Since there is still enough energy in the system, the hammer moves again out of the measuring length of the sensor until it falls again into its measuring length. After a while, when the ice specimen fails, the measurement is cut to save memory. The third graph shows the force-time section between the time of the first local maxima and the second local minima of the unprocessed displacement-time measurement. However, the time window still needs to be bigger for a good resolution of the impact scenario. Thus the fourth graph shows a more detailed representation of the impact scenario. The numbers in the fourth graph indicate when the high-speed camera took pictures from the failure process, see later Figure 7. This test is also put into context with the other tests in Figure 6, represented as a force-displacement curve.

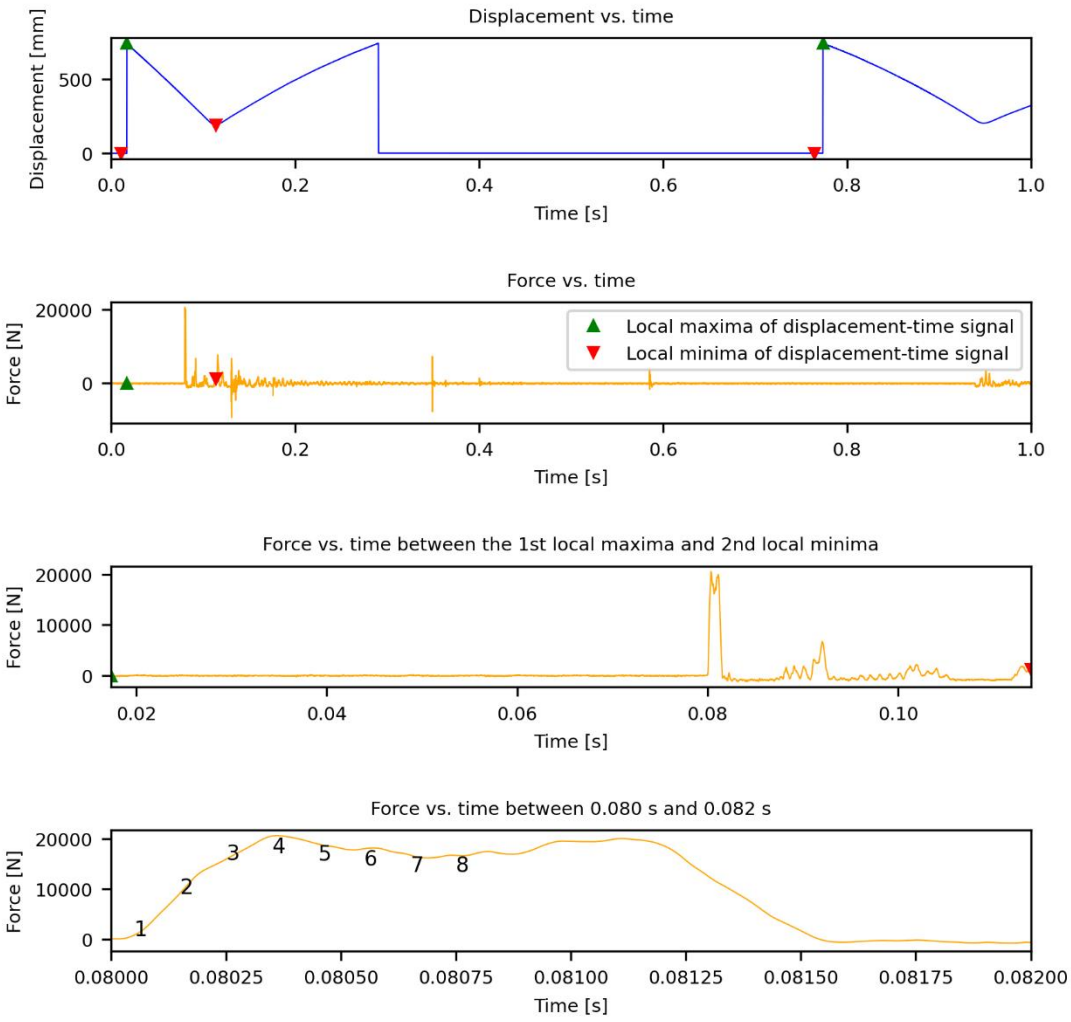

Figure 2: Detailed view of the measurements during the tests at maximum nominal velocity with steel-ice contact

Figure 3 shows the same four graphs for the test at maximum nominal impact velocity with rubber-ice contact. The numbers in the fourth graph indicate the selected pictures of the failure process from the high-speed recording, see later Figure 8. Here the authors selected four pictures at the start where the measured load increased and further four pictures where the maximum measured load was reached, as in between the selection, the pictures were hard to distinguish from the presented ones and thus did not provide any additional value for the description of the failure process. This test is also put into context with the other tests in Figure 6, represented as a force-displacement curve.

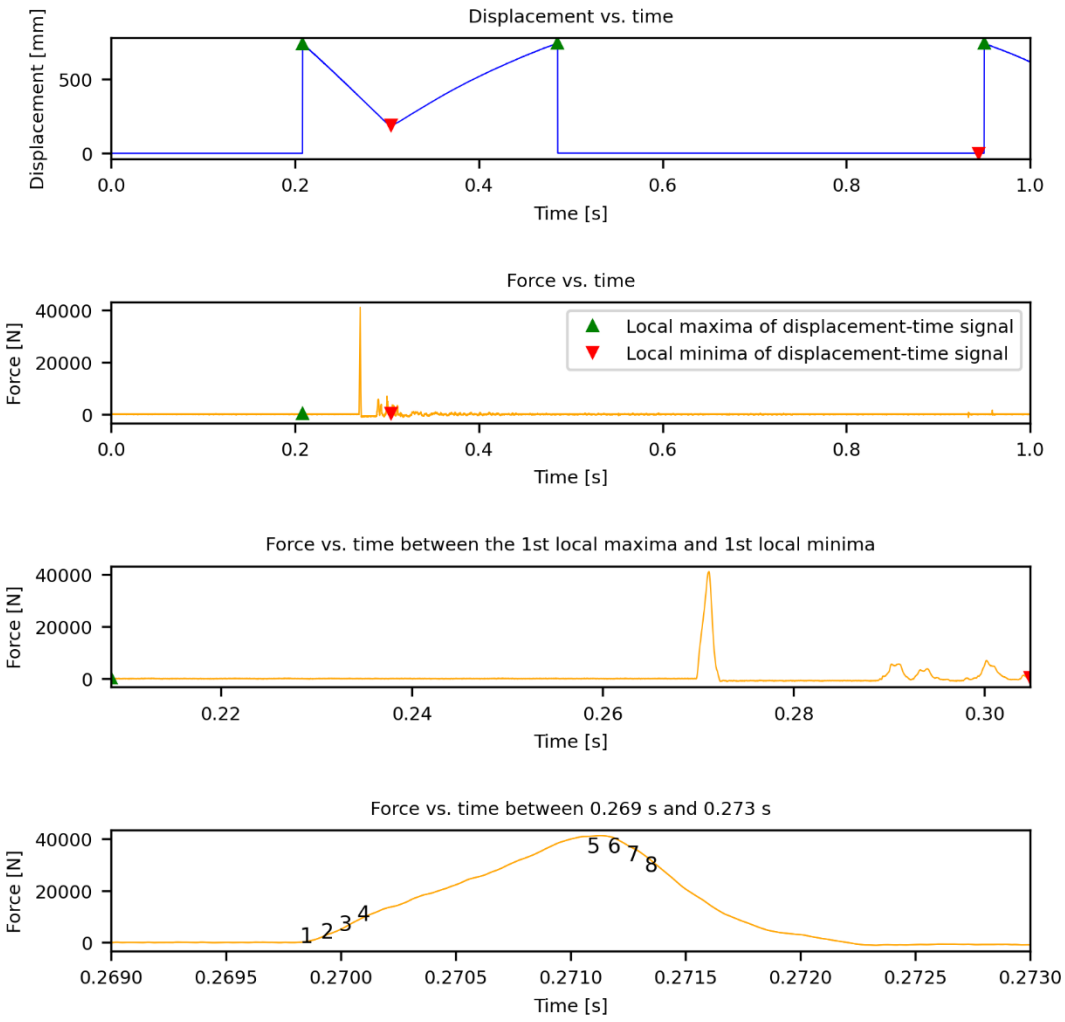

Figure 3: Detailed view of the measurements during the tests at maximum nominal velocity and rubber-ice contact

In Figure 4, the force is plotted against the displacement after the first contact for the tests with a nominal velocity of 3,132 mm/s. On the left side is the plot for the steel-ice end-cap conditions next to the tests with the rubber-ice end-cap conditions on the right side of Figure 4. For both test series, five repetitions were conducted. The maximum measured displacement is between 4-10 mm, while the maximum measured force is between 10-30 kN for the tests with the steel-ice end-cap conditions. For the rubber-ice conditions, the maximum measured displacement is between 8-10 mm, and the maximum measured force is between 80-110 kN. Compared to the tests with the steel-ice end-cap conditions, the curves of the tests with the rubber-ice end-cap conditions are less scattered.

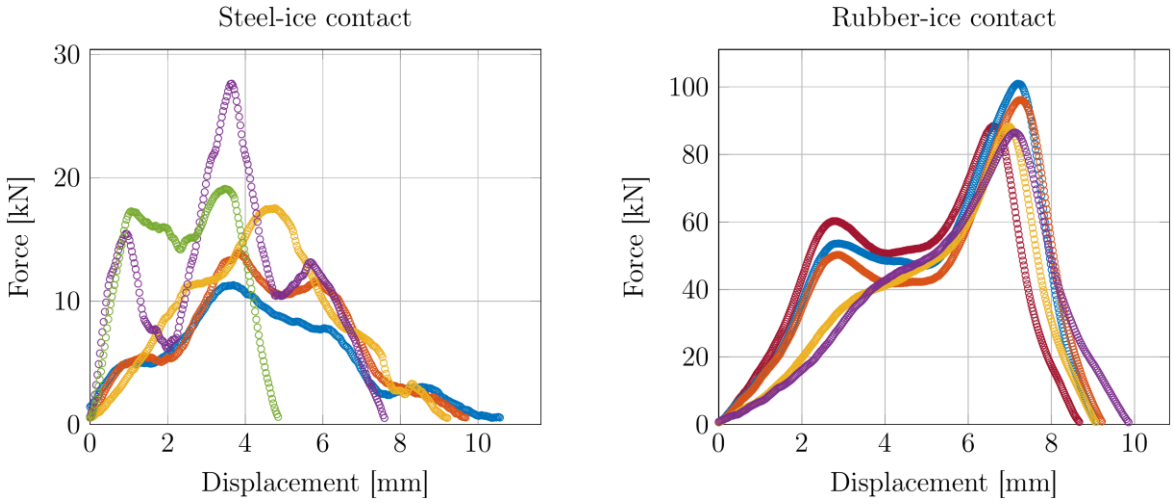

Figure 4: Force-displacement curves for the drop tower tests at v_n = 3,132 mm/s; left steel-ice contact; right rubber-ice contact

Figure 5 shows five force-displacement curves for the steel-ice tests with a nominal velocity of 5,425 mm/s on the left side, besides 14 rubber-ice tests on the right side of Figure 5. For the steel-ice tests with the higher impact velocities, the scatter is reduced compared to those with a nominal velocity of 3,132 mm/s, see Figure 4. The global maximum is between 10 and 30 kN and the maximum measured displacement is between 7 mm and 14 mm. The curves on the right side of Figure 5 are narrow bell-shaped. For the tests with a nominal velocity of 5,425 mm/s and with the rubber-ice end-cap conditions, the maximum measured displacement is between 10-14 mm, and the maximum measured force is between 50-110 kN.

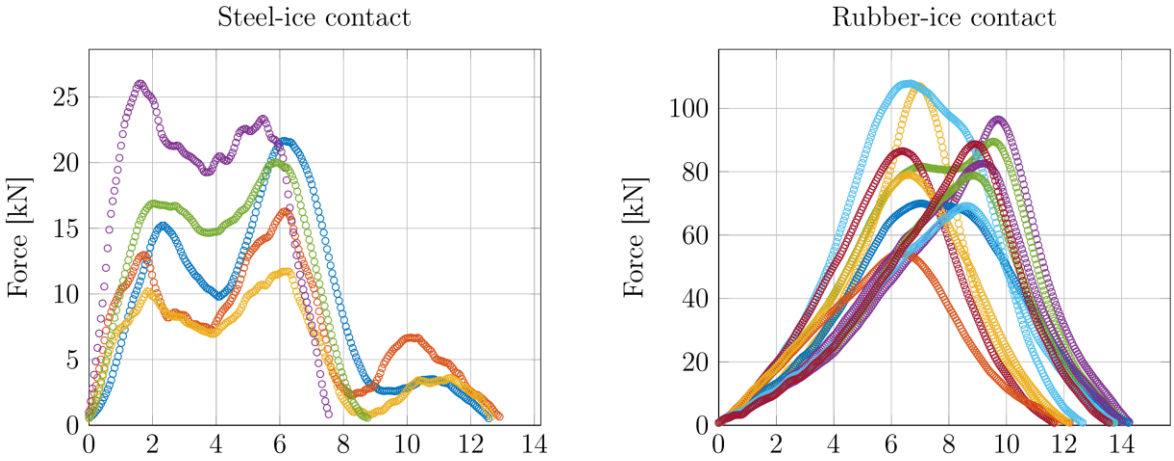

Figure 5: Force-displacement curves for the drop tower tests at v_n = 5,425 mm/s; left steel-ice contact; right rubber-ice contact

On the left side of Figure 6, five force-displacement curves for the tests with a nominal velocity of 6,185 mm/s and steel-ice end-cap conditions are shown. Next to these curves, 14 tests with the rubber-ice end-cap conditions are shown on the right side of Figure 6. For the steel-ice tests with the highest impact velocities, the scatter is less than those with a nominal velocity of 5,425 mm/s, see Figure 5. The maximum measured force is 15-25 kN, and the maximum measured displacement is 8-14 mm. On the right side of Figure 6, the curves are again narrow bell-shaped. However, the scatter is more notable for the 6,185 mm/s tests than

those with a nominal velocity of 5,425 mm/s, see Figure 5. The maximum measured displacement is 10-20 mm, and the maximum measured force is 20-120 kN.

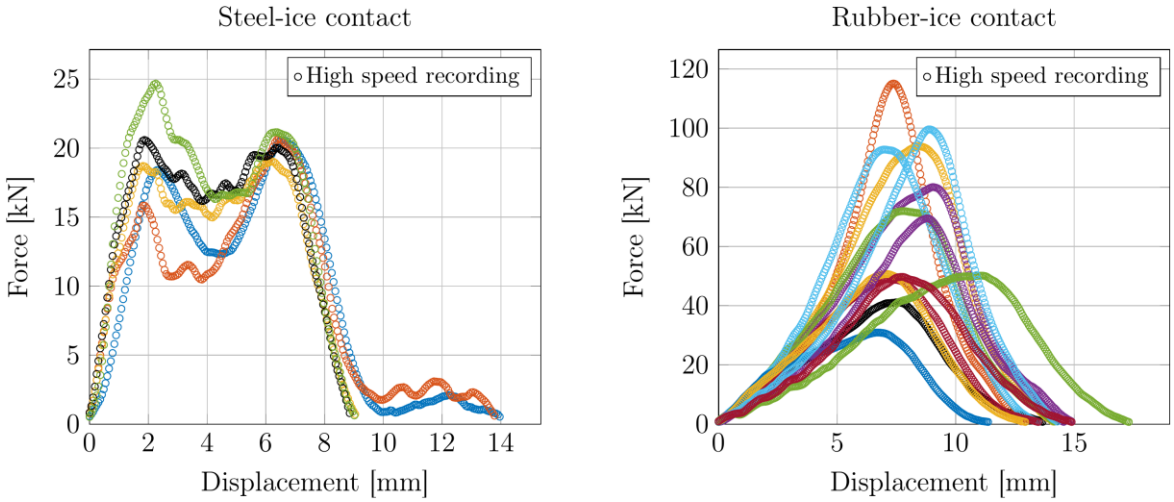

Figure 6: Force-displacement curves for the drop tower tests at v_n = 6,185 mm/s; left steel-ice contact; right rubber-ice contact

High-speed recordings

The failure behavior of the ice was recorded for all tests with few exceptions where the camera was not appropriately triggered or was out of focus. The current section shows the best pictures representing each of the end-cap conditions ordered from left to right and from top to bottom. The according measurements were shown in detail in Figure 2 and Figure 3.

Figure 7 shows the failure behavior of a test with steel-ice end-cap conditions tested at a nominal velocity of 6,185 mm/s. Pictures were taken at 10,000 fps, and the authors selected only the first eight pictures (see Figure 2) since the following pictures did not provide any additional value to the description of the failure process. The first picture shows the intact ice specimen. After the hammer has contact with the ice specimen, the defects increase rapidly until several axial cracks develop, see the second to fourth picture in Figure 7. The red circle indicates the first visible crack at the top and the emergence of an axial crack (pictures 3-4). The number of cracks increases and starts to be visible at the bottom of the specimen (pictures 5-7) until the specimen crushes at the top at the hammer location, see picture 8. Independent of the nominal velocity, the ice specimen failed by crushing at the top in every recorded test with steel-ice end-cap conditions.

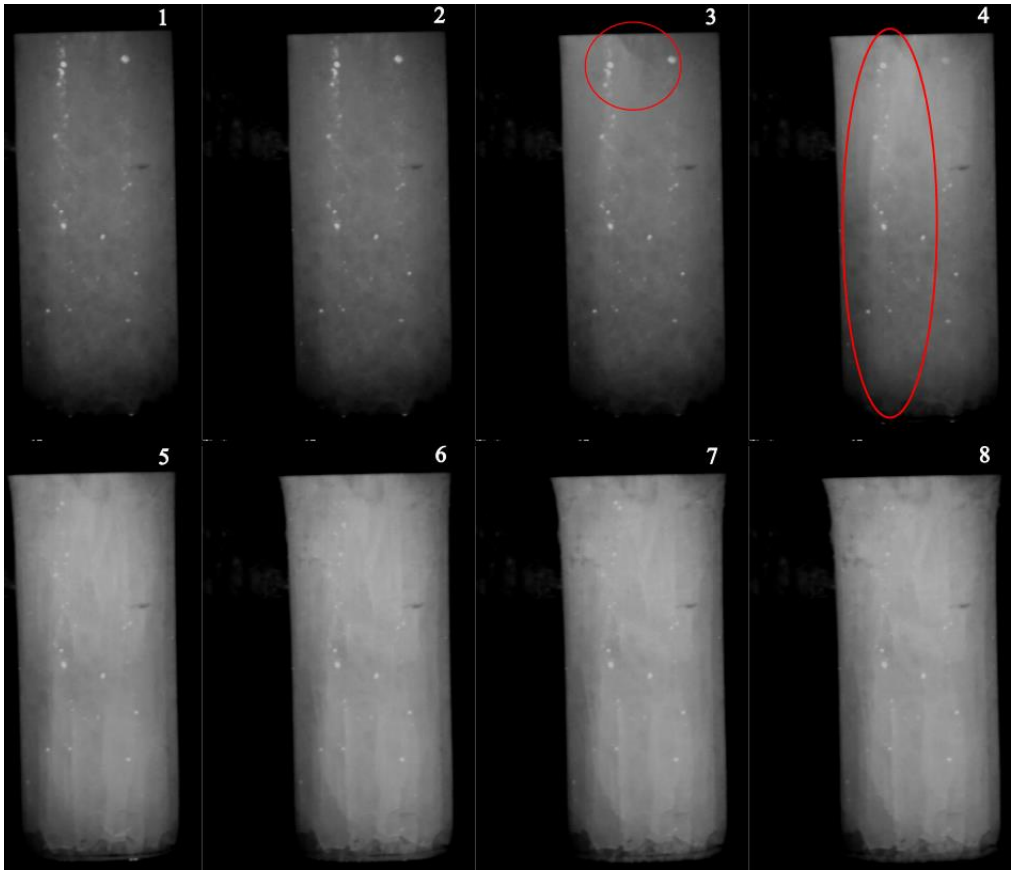

Figure 7: Failure behavior of the ice specimen tested at a nominal impact velocity of 5,425 mm/s with steel-ice contact conditions

Figure 8 shows the failure behavior of a test with rubber-ice end-cap conditions tested at a nominal velocity of 6,185 mm/s. Here the pictures were taken at 12,000 fps. The first picture shows the intact ice specimen. The second picture shows an axial crack at the top of the specimen (red circle). The fourth picture shows the development of a wing crack (red circle). Compared to Figure 7 (pictures 1-4), fewer defects develop, and the cracks are more located in the middle of the specimen when testing with rubber-ice end-cap conditions. In the last four pictures of Figure 8, the specimen fails at the wing crack location, and the specimen displaces along the wing crack. In the pictures in between the selection (time between picture 4 and picture 5), it was notable that the specimen moved in the vertical direction. The presented failure behavior was observed for some tests with rubber-ice end-cap conditions. Instead, most ice specimens failed at the top or bottom, and some failed at the middle for the test with rubber-ice end-cap conditions.

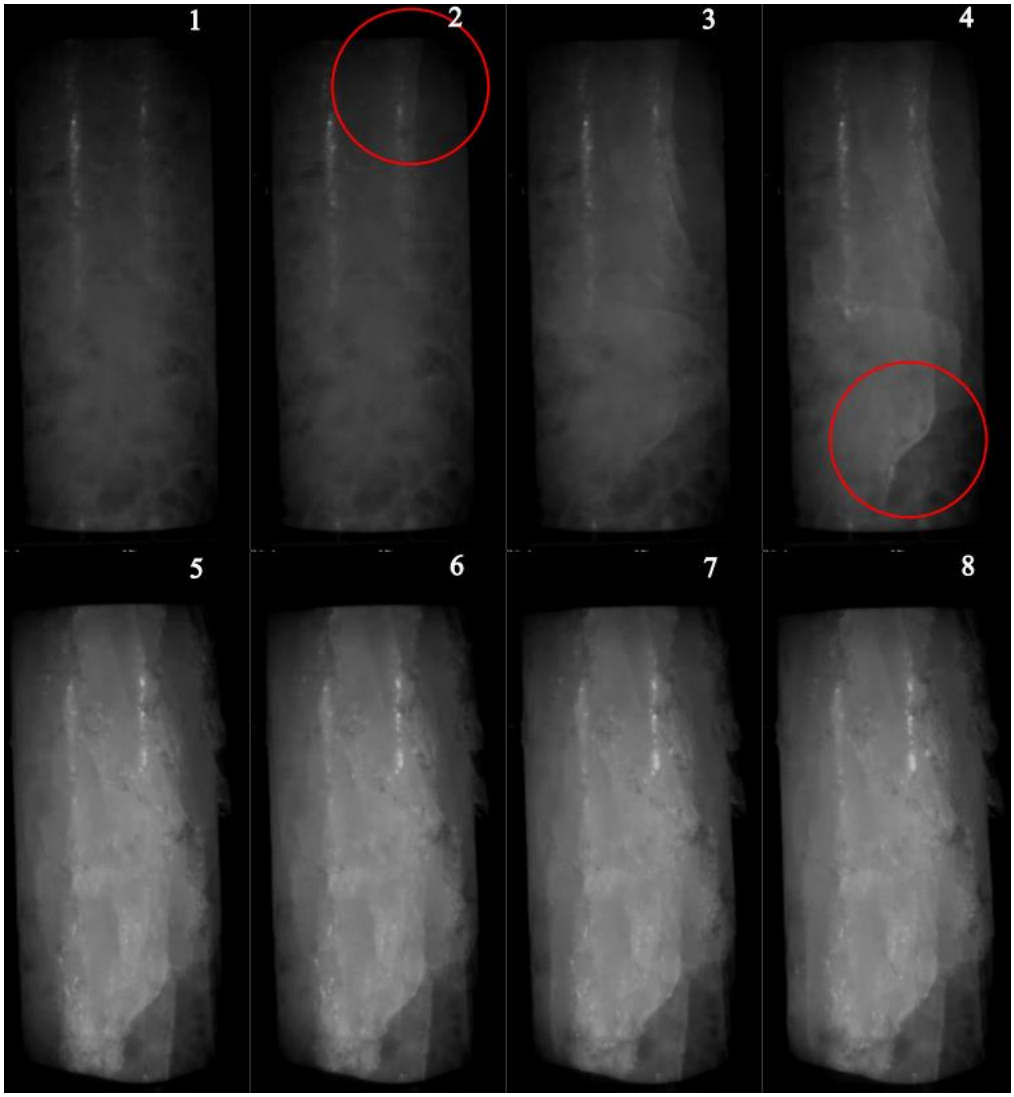

Figure 8: Failure behavior of the ice specimen tested at a nominal impact velocity of 6,185 mm/s with rubber-ice contact conditions

Analysis

In the processing of the data the displacement values were cut where the hammer falls into the possible measuring length of the displacement sensor and stores the corresponding time, force, and displacement measurements until the force measurements return to zero. The impact velocity is determined by fitting a second-order polynomial curve to the cut displacement and cut time measurements and deriving the resulting curve. The velocity is evaluated at the time step where the hammer has initial contact with the ice specimen. The measured peak force divided by the initial cross-section defines the compressive pressure. Table 2 shows the results of the tests. Next to the nominal velocity (v_n), the mean measured velocity (v_m), the standard deviation of the measured velocity (v_{std}), the mean measured compressive pressure (σ_c), and the standard deviation of the measured compressive pressure (σ_{std}) is displayed.

Table 2. Test results

End-cap condition	No. of tests	v_n [mm/s]	v_m [mm/s]	v_{std} [mm/s]	σ_c [MPa]	σ_{std} [MPa]
Steel-ice	5	3,132	3,016	25.2	2.307	0.719
Steel-ice	5	5,425	5,259	12.8	2.466	0.626
Steel-ice	5	6,185	5,999	34.5	2.719	0.243
Rubber-ice	5	3,132	2,755	137.7	9.312	2.112
Rubber-ice	14	5,425	5,015	101.9	9.940	2.843
Rubber-ice	14	6,185	5,806	97.9	8.520	3.332

For the tests with the steel-ice end-cap conditions, the mean measured velocity is lower than the nominal velocity (Ø -156 mm/s) and has a relatively low standard deviation. The mean measured velocity for the tests with the rubber-ice end-cap conditions is also lower than the nominal velocity (Ø -389 mm/s). In contrast to the steel-ice test series, the standard deviation of the mean measured velocity in the rubber-ice test series is bigger. With increasing drop heights, the standard deviation of the mean measured velocity gets lower in the tests with the rubber-ice end-cap conditions. In contrast, the standard deviation in the steel-ice end-cap condition seems more random.

The mean measured compressive pressure increases from 2.307 MPa to 2.719 MPa with the increasing test interaction velocities for the steel-ice end-cap conditions, whereby the standard deviation of the mean measured compressive pressure decreases. For the tests with the rubber-ice end-cap conditions, the mean compressive strength is 9.312 MPa for the nominal velocity of 3,132 mm/s, 9.940 MPa for the nominal velocity of 5,425 mm/s and 8.520 MPa for the nominal velocity of 6,185 mm/s. The standard deviation of the measured compressive pressure increases with increasing interaction velocities.

For comparison, the results of the present study are shown in Figure 9, besides compression tests of ice with steel-ice and rubber-ice contact, which were previously conducted (Böhm *et al.*, 2022a, 2022b). Figure 9 summarizes the measured compressive strength of the conducted ice tests over the strain-rate. The strain-rate is the velocity divided by the initial length of the specimen. The strain-rate is displayed in a logarithmic scale, and the trend line for freshwater ice tested under compression at -10 °C is from Jones (2007). For the compression tests of ice, the ice specimens had the exact dimensions as in this study, but the testing temperature was different. The test temperature of the compression tests was -10 °C, whereas the drop tower tests were conducted at an ambient temperature. Jones (2007) gives a trend line for each behavior, ductile or brittle. The tests in the ductile range (strain-rate up to 10^{-3} s^{-1}) lay at or above the trend line. For strain-rates beyond 10^{-3} s^{-1} the behavior of the ice changes from ductile to brittle. Due to the complexity of the failure mechanism, more scatter of the data is expected. The compression tests of ice at the brittle range lay below the trend line. Compression tests with rubber-ice contact resulted in lower compressive strength values in the ductile range than those with steel-ice contact. This pattern changes for the tests in the brittle range, where the strength values are higher for the tests with the rubber-ice contact - all specimens tested with rubber-ice contact conditions in the compression test failed by axial splits.

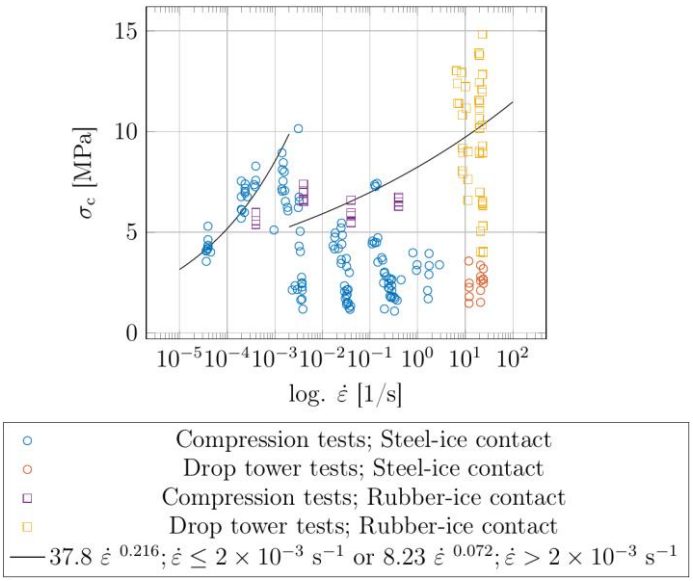

Figure 9: Compressive strength measured in compression tests of ice besides drop tower tests of ice over the strain rate

DISCUSSION

Multi-year sea ice is typically less saline, resulting in low porosity and greater strength than first-year sea ice, thus making the multi-year ice more similar to freshwater and glacial ice (Timco & Weeks, 2010). However, multi-year sea ice has a variety of mixed grain structures. In the presented study, the specimen preparation took place at -10 °C, and the resulting granular ice specimens were tested under ambient temperature (around 20 °C). Due to the fast processing and test execution (within 5 min), it is reasonable to assume that the ice specimens had a slightly higher temperature of around -10 °C during the impact. Due to the size of the drop tower, the tests are only possible under ambient conditions. Nevertheless, impact tests at lower temperatures result in higher measured strength values (Wu & Prakash, 2015), although there is much literature on ice testing at temperature of -10 °C (Kellner, 2022).

In compression tests or impact tests of brittle materials, it is exceedingly difficult to produce a uniform uniaxial stress field, and compliant plates were recommended as compensation for the lack of flatness on the sample ends (Hawkes & Mellor, 1970; Hawkes & Mellor, 1972; Haynes & Mellor, 1977; Schwarz *et al.*, 1981). The present study showed that 3 mm rubber plates alleviate problems like end flatness and lack of parallelism to such a degree that the measured ice strength is more than three times higher than drop tower tests without these plates (see Table 2). The high-speed recordings of the present study show that the ice specimens failed by axial splitting and crushing at the local impact location when tested with steel-ice contact conditions (see Figure 7) and showed a slight increase of the compressive strength with increasing strain-rates (see Table 2). The recordings of the rubber-ice contact conditions showed a mixture of fracture types. On a few recordings of the rubber-ice contact conditions, wing cracks (shear faulting) could be observed (see Figure 8), which was not observed before in the literature for strain-rates from 12 s^{-1} to 24 s^{-1}. This change in failure modes and, thus, in measured strength supports the statement from Schulson (1987; Schulson *et al.*, 1989; Schulson, 1990). The increase of the compressive strength with increasing strain-rates is not that clear for the presented drop tower tests with rubber plates

because the compressive strength measurements showed an initial increase from the lowest impact velocity to the subsequent higher impact velocity. However, a subsequent drop in the measured strength was observed for the highest impact velocity.

Cole (1987) reported for uniaxial ice testing in the strain-rate range of 10^{-2} to 10^{-1} that the measured strength is independent of the strain-rate. Comparing this observation to the study of Hawkes and Mellor (1972), this could result from high tolerances at the surface of the specimen ends and at the platen surface, which caused an apparent decrease in compressive strength during ice compression tests in the brittle range. The previously conducted compression tests of ice at the *Hamburg University of Technology* support this conclusion (Böhm *et al.*, 2022b, 2022a). The strength decreased in the range of 10^{-2} to 10^{-1} s^{-1} for the compression tests of ice with steel-ice contact condition (< 5 MPa). Nevertheless, the compression tests of ice with rubber-ice contact conditions revealed a strain-rate dependency of the measured compressive strength (> 5 MPa). The tested strain-rates lie between the tested strain-rates of Jones (1997) and Fasanella *et al.* (2006), and together with the findings from Shazly *et al.* (2009), a positive strain-rate dependency of the measured strength could be observed. Shazly et al. (2009) found the effect of specimen end-constraint negligible for uniaxial compression testing of ice using a modified split Hopkins pressure bar, and for drop tower tests with ice, the present study found the effect of specimen end-constraint to be significant. However, the comparability of the results and findings due to the different testing setups and methods is rarely given.

Furthermore, recordings of the failure process increased the interpretability of the test results. For the range of tested velocities, a frame rate of 10,000 fps was sufficient, but the authors suggest ten times higher frame rates. In addition, the precise point of time where the pictures were taken (numbers in the last graph) could not be determined as the high-speed recordings, and the measurements were not synchronized. But the possible deviation of the numbers in Figure 2 and Figure 3 is at least the distance between the points. In addition, numbers lie more to the left in the time than indicated in Figures 2 and 3 because the contact between the hammer and ice specimen happens before the load cells can measure the system's reaction. The rubber plates in this study were changed every 2-3 test runs but the plates should be changed for every test run since the rubber plates seem to harden after the test. The hardening effect of the rubber plates, the irregular exchange of the rubber plates, and the double-sided tape's influence could result in the increased standard deviation of the mean measured compressive strength. Despite the number of repetitions, the influence of the rubber plates is studied more quantitative than qualitative. In hindsight, using spherically-seated compression platens to accommodate the angular displacement of the top of the specimen with reference to the loading axis and lapping the specimen's ends providing a final smooth finish is believed to improve the testing method as the friction between steel and ice resembles more to the friction in propeller-ice interaction. The platens should be able to self-aligning in the dynamic range. In addition, spherically-seated compression platens are typically used with a fixed-plane platen. However, the rubber plate's merit lies in the way it leads to a simple treatment of surface irregularities at the specimen's end and misalignment to the impact plate.

In addition, determining the impact velocity or strain-rate for testing is debatable. Here, the velocity calculation based on the displacement measurement is described, besides determining the nominal impact velocity. The impact velocity is essential, e.g., for calculating an initial engineering strain-rate. The engineering strain-rate is commonly used for strain-rate-dependent materials like ice. The problem in calculating the velocity of

displacement measurements is that there must be a standardized procedure. But the velocity can differ depending on the method for the determination of the velocity. In the present study, the time step, where the velocity is determined, influence the calculated velocity. Thus, the mean measured velocity serves more as an orientation and should not be used to describe the influence of the rubber plates on the measured velocity. Nevertheless, rubber plate usage is expected to reduce the applied strain-rate. In addition, after the hammer contacts the specimen, the velocity decreases, which is a significant difference from compression tests where ideally, the velocity is kept constant until the failure of the specimen.

CONCLUSION

Drop tower tests of cylindrical granular ice specimens (D = 99.4 mm, L = 250 mm) show a strain-rate dependency (12 s^{-1} – 24 s^{-1}) of the nominal compressive strength and a dependency of the applied boundary conditions on the failure mode. This indicates a high sensitivity of the ice strength and the exerted forces by the ice in dependence on the stiffness or compliance of the interacting structure. Regarding the findings of this paper, the development of suitable holistic numerical ice material models for propeller-ice interaction simulations needs to consider the boundary conditions, the stiffness of the interacting structure, the failure mode of the ice, and the strength dependencies of the ice on the strain-rate.

ACKNOWLEDGEMENTS

The authors would like to acknowledge support from MarTERA - an ERA-NET Cofund scheme of Horizon 2020 of the European Commission - and the Research Council of Norway (Project no. 311502), the Federal Ministry for Economic Affairs and Climate Action of Germany (Project no. 03SX519B), and Department of Science and Technology of South Africa, through the HealthProp project. Further this work was supported by the US Office of Naval Research Global (ONRG) under NICOP Grant N62909-22-1-2019. It is stated that the funder is not responsible for any of the content of this publication.

References

Böhm, A.M., Herrnring, H. & Bock Und Polach, F. von (2022a) Data from uniaxial compressive testing of laboratory-made granular ice. *Data in Brief*, 42, 108236. Available from: https://doi.org/10.1016/j.dib.2022.108236.

Böhm, A.M., Herrnring, H. & Bock Und Polach, F. von (2022b) Lessons Learned: The Influence of Testing Properties on Uniaxial Compression Tests of Ice. In: *Volume 6: Polar and Arctic Sciences and Technology, ASME 2022 41st International Conference on Ocean, Offshore and Arctic Engineering,* 5-10 June, Hamburg, Germany. American Society of Mechanical Engineers.

Cole, D.M. (1987) Strain-Rate and Grain–Size Effects in Ice. *Journal of Glaciology*, 33(115), 274–280. Available from: https://doi.org/10.3189/S0022143000008844.

Fasanella, E.L., Boitnott, R.L. & Kellas, S. (2006) *Dynamic Crush Characterization of Ice*. NASA.

Gudimetla, P.S.R., Colbourne, B., Daley, C., Bruneau, S.E. & Gagnon, R. (2012) Strength and Pressure Profiles of Conical Ice Crushing Experiments. In: *Day 2 Tue, September 18, 2012, SNAME 10th International Conference and Exhibition on Performance of Ships and Structures in Ice,* 17-20 September, Banff, Alberta, Canada. SNAME.

Hawkes, I. & Mellor, M. (1970) Uniaxial testing in rock mechanics laboratories. *Engineering Geology*, 4(3), 179–285. Available from: https://doi.org/10.1016/0013-7952(70)90034-7.

Hawkes, I. & Mellor, M. (1972) Deformation and Fracture of Ice Under Uniaxial Stress. *Journal of Glaciology*, 11(61), 103–131. Available from: https://doi.org/10.3189/S002214300002253X.

Haynes, F.D. & Mellor, M. (1977) Measuring the Uniaxial Compressive Strength of Ice. *Journal of Glaciology*, 19(81), 213–223. Available from: https://doi.org/10.3189/S0022143000029294.

Jones, S.J. (1997) High Strain-Rate Compression Tests on Ice. *The Journal of Physical Chemistry B*, 101(32), 6099–6101. Available from: https://doi.org/10.1021/jp963162j.

Jones, S.J. (2007) A review of the strength of iceberg and other freshwater ice and the effect of temperature. *Cold Regions Science and Technology*, 47(3), 256–262. Available from: https://doi.org/10.1016/j.coldregions.2006.10.002.

Kellner, L. (2022) *Analyzing the complexity of ice with explainable machine learning for the development of an ice material model*. TUHH Universitätsbibliothek. Available from: https://doi.org/10.15480/882.4076.

Schulson, E. (1987) The Fracture of Ice Ih. *Le Journal de Physique Colloques*, 48(C1), C1-207-C1-220. Available from: https://doi.org/10.1051/jphyscol:1987129.

Schulson, E. (1990) The brittle compressive fracture of ice. *Acta Metallurgica et Materialia*, 38(10), 1963–1976. Available from: https://doi.org/10.1016/0956-7151(90)90308-4.

Schulson, E.M., Gies, M.C., Lasonde, G.J. & Nixon, W.A. (1989) The Effect of the Specimen–Platen Interface on Internal Cracking and Brittle Fracture of Ice Under Compression: High-Speed Photography. *Journal of Glaciology*, 35(121), 378–382. Available from: https://doi.org/10.3189/S0022143000009308.

Schwarz, J., Frederking, R., Gavrillo, V., Petrov, I.G., Hirayama, K.-I. & Mellor, M. et al. (1981) Standardized testing methods for measuring mechanical properties of ice. *Cold Regions Science and Technology*, 4(3), 245–253. Available from: https://doi.org/10.1016/0165-232X(81)90007-0.

Shazly, M., Prakash, V. & Lerch, B.A. (2009) High strain-rate behavior of ice under uniaxial compression. *International Journal of Solids and Structures*, 46(6), 1499–1515. Available from: https://doi.org/10.1016/j.ijsolstr.2008.11.020.

Soininen, H. (1998) *A propeller-ice contact model*. VTT: Espoo.

Timco, G.W. & Weeks, W.F. (2010) A review of the engineering properties of sea ice. *Cold Regions Science and Technology*, 60(2), 107–129. Available from: https://doi.org/10.1016/j.coldregions.2009.10.003.

Veitch, B. (1995) *Predictions of ice contact forces on a marine screw propeller during the propeller ice cutting process*. Finnish Acad. of Technology: Helsinki.

Wu, X. & Prakash, V. (2015) Dynamic compressive behavior of ice at cryogenic temperatures. *Cold Regions Science and Technology*, 118, 1–13. Available from: https://doi.org/10.1016/j.coldregions.2015.06.004.